European Commission

Horizon 2020
European Union funding
for Research & Innovation

Horizon 2020 Grant Agreement Number 734798

indoor small-cell Networks with 3D MIMO Array Antennas (is3DMIMO)

D2.2
Report on the impact of measurement uncertainties of array antennas in RIMP and RLOS and their impact on 3D SMX and 3D beamforming performance

Authors(s)	Andrés Alayón Glazunov, Jian Yang, Jiliang Zhang, Sadegh Mansouri Moghaddam, Yang Wang
Author(s) Affiliation	University of Twente, Netherlands; Chalmers University of Technology, Sweden; Lanzhou University, P. R. China; Harbin Institute of Technology, Shenzhen Graduate School, P. R. China.
Editor(s):	Andrés Alayón Glazunov
Status-Version:	Final-1.0
Project Number:	734798
Project Title:	indoor small-cell Networks with 3D MIMO Array Antennas (is3DMIMO)
Project Acronym:	is3DMIMO
Work Package Number	2

Abstract Over-the-Air (OTA) measurements and characterization of Massive Multiple-Input Multiple-Output (MIMO) antenna systems for 5G have to be time- and cost-efficient. Two potential measurement candidates are OTA measurement environments emulating (1) the Rich Isotropic MultiPath (RIMP) and (2) the Random Line-Of-Sight (RLOS) channels. In this deliverable, we present the MIMO efficiency characterization of single-User MIMO (SU-MIMO) systems. In addition, we present a study of the capacity loss of downlink Massive MIMO narrowband systems in RIMP/RLOS due to deficiently performing antenna elements. We consider the downlink ergodic sum-rate capacity loss for the Zero-Forcing (ZF) and the Matched-Filtering (MF) precoders in these channels. Assumed is a single-cell system comprising a base station with 50 equidistant isotropic source antenna elements placed $\lambda/2$ apart and 5 users each equipped with a single isotropic antenna. No mutual coupling effects between the elements of an array are assumed. In the present study we show that both the RIMP and the RLOS can be used to identify deficient performance of Massive MIMO arrays and analyze the detrimental impact of deficient and or erroneous antennas Massive MIMO performance.

The results presented in this deliverable have addressed the requirement of Task 2.2 in the is3DMIMO project. In the future, more results will be delivered to contribute to the comparison of the 3D SMX and 3D beamforming performance obtained under the indoor 3D spatial channel model extended (SCME) MIMO channel model established in Task 1.2 and that under the measured indoor 3D MIMO channel in Task 1.3.

Keywords: MIMO efficiency, sum-rate capacity, deficient antenna,Massive MIMO capacity loss, OTA, RIMP, RLOS

Table of Contents

Index of Figures

1   Introduction

5G wireless systems will bring an abundance of quality-of-service enhancements to the end-user, such as user throughput at the Gbps order-of-magnitude, sub-millisecond latency, as well as better link reliability and larger coverage and capacity. One of the key technologies in 5G wireless networks is Massive MIMO (Massive Multi-User Multiple-Input Multiple-Output), where a radio base stations (RBS) or access point (AP) are supplied with array antennas. Each array is comprised by a huge number of antenna elements, and can serve many users in the same time-frequency resource. In so-called favorable propagation (FP) conditions, the channel vectors between the users and the RBS are nearly pairwise orthogonal. Hence, linear signal processing becomes nearly optimal and the RBS can use linear receivers in the uplink and linear precoders in the downlink [1, 2].

Channel models are essential to characterize the performance of wireless systems. The so-called Rich Isotropic Multipath (RIMP) propagation channel and the Random Line-Of-Sight (RLOS) propagation channel represent two limiting propagation channels in terms of spatial distribution of incoming and outgoing waves at an antenna. These channels have been proposed to develop time- and cost-efficient OTA (Over-The-Air) characterization set-ups. The main idea is based on the *Kildal-conjecture* for OTA device characterization [8]: *if a wireless device is proven to work well in RIMP and RLOS, it will work well in all real-life channels in a statistical sense.* Analogous ideas have been proposed later in the context of Massive MIMO systems too in [3, 4], concluding that both these channels provide FP conditions. Hence, suggesting that real propagation channels, which are expected to be in between the extremes, would also provide FP conditions. Real-life channel sounding measurements of FP characteristics of Massive MIMO have been reported, e.g., in [5].

It is worthwhile to note that the RLOS propagation channel is a generalization of the pure LOS channel, where the randomness arises from the unpredictable user positions and orientations of their antennas, or the position deployment of a RBS or AP. In RLOS, both the Angle-of-Arrival (AoA) and the polarization of the LOS wave can be considered to be random variables depending on the specific application.

Based on the above we can conclude that the RIMP and the RLOS channels can provide a practical approach to the OTA characterization of Massive MIMO devices, e.g., RBSs, APs, mobile phones, etc., in 5G wireless systems. Their relevance is further accentuated by the fact that 5G massive array antennas will, in practice, be only possible to measure in OTA set-ups due to the large number of ports. Moreover, as we go higher in frequency, e.g., for systems operating at the millimeter waves there will be most likely

no access to the antenna (or measurement) ports.

Hence, to detect insufficient performance of large array antennas is one of the key objectives of OTA characterization of MIMO antenna systems. In this deliverable, we first present an analysis of the MIMO efficiency performance of antenna in single-user MIMO (SU-MIMO) to detect antenna deficiency in a wireless channel that can be emulated in an OTA set-up [6]. Secondly, we present simulation results of the impact of deficient antennas in terms of the capacity loss of downlink Massive MIMO narrowband systems in the RIMP and the RLOS channels [7]. Equivalently, this can be seen as the impact of measurement errors (uncertainties) on the Massive MIMO performance. More specifically, we assume that some of the antennas have a total embedded radiation efficiency that is less than 100%, or equivalently, that there are measurement errors associated with each antenna element. The achievable ergodic sum-rate capacity of a downlink Massive MIMO system is evaluated for the Zero-Forcing (ZF) and the Matched-Filtering (MF) linear precoders.

2 SU-MIMO

2.1 System Model

Let's first assume a single-user multiple-input multiple-output (SU-MIMO) system with N_r receive antennas and N_t transmit antennas, $\min\{N_r, N_t\}$ parallel data streams can be produced. The signals received by a multi-port antenna can be modelled by the following input-output relationship

$$\mathbf{y} = \mathbf{H}\mathbf{x} + \mathbf{n}, \tag{1}$$

where $\mathbf{y} \in \mathbb{C}^{N_r \times 1}$ and $\mathbf{x} \in \mathbb{C}^{N_t \times 1}$ are the receive and transmit signal vectors, respectively; $\mathbf{H} \in \mathbb{C}^{N_r \times N_t}$ is the channel matrix, and $\mathbf{n} \in \mathbb{C}^{N_t \times 1}$ is the additive white Gaussian noise (AWGN) vector of i.i.d. (independent identically distributed) Gaussian-distributed variables with zero-mean.

Considering an open-loop MIMO system, i.e., no channel state information is available at the transmitter, the Zero-Forcing (ZF) algorithm can be employed to provide for spatial multiplexing. The ZF-algorithm involves computing the pseudo-inverse matrix of the channel matrix, i.e.

$$\mathbf{y}^{\text{ZF}} = \mathbf{H}^{+}\mathbf{y}, \tag{2}$$

where $\mathbf{H}^{+} = \left(\mathbf{H}^{H}\mathbf{H}\right)^{-1}\mathbf{H}^{H}$, $\mathbf{H}^{H}$ and $\mathbf{H}^{-1}$ denote the Penrose pseudo-inverse, the Hermitian matrix transpose and the matrix inverse operations performed on matrix $\mathbf{H}$, respectively. ZF-algorithm results in a nulling of the interference from the yet undetected

streams at the expenses of enhancing the noise. The SNR of the jth data stream can be expressed as

$$\gamma_j^{\text{ZF}} = \frac{\gamma_j}{\left[(\mathbf{H}^H\mathbf{H})^{-1}\right]_{j,j}}, \tag{3}$$

where $\gamma_j = E\left[|x_j|^2\right]/E\left[|n_j|^2\right]$ and $[\mathbf{H}]_{j,j}$ the jth diagonal element of the matrix $\mathbf{H}$.

The entries of the channel matrix $\mathbf{H}$ in (1) are proportional to the voltages induced at the ports of the receive antenna. The electromagnetic (EM) field impinging at the receive antenna is the outcome of the influence of the propagation channel on the EM field radiated by the transmit antenna. An ideal 2-port antenna with 100% embedded efficiency and orthogonally polarized far-field functions and equal gain over the unit sphere is assumed for reference. The embedded far-field function of the antenna element n is given by the vector-function $\boldsymbol{F}_n$. Its further assumed that antenna elements at the receive array - e.g., at an RBS, and the transmit array - e.g., the user equipment (UE), are in the far-field of each other. The field impinging at the receive antennas is assumed to consist of the superposition of linearly polarized plane waves coming from one hemisphere. [8,9].

2.2 The RLOS channel

In the RLOS propagation channel, the maximum degrees of freedom equals 2 for closely spaced antennas due to the possibility to produce two orthogonal polarizations. Hence, the coupling between the two antennas can be computed as

$$H_{n,m}^u = c\boldsymbol{F}_n(\theta^u, \phi^u) \cdot \hat{\boldsymbol{p}}_m^u, \tag{4}$$

where $c = 1$ given the assumed reference antenna mentioned above. Denoting the angles-of-arrival (AoA) in spherical coordinates (θ^u, ϕ^u), the polarization vectors of the two waves impinging waves are given by

$$\hat{\boldsymbol{p}}_m^u = \sin(\alpha^u + (m-1)\frac{\pi}{2})\hat{\boldsymbol{\theta}} + \cos(\alpha^u + (m-1)\frac{\pi}{2})\hat{\boldsymbol{\phi}}, \tag{5}$$

where $m \in \{1, 2\}$ is the index denoting either of the two orthogonal polarizations. The superscript u is used to denote a random realization of the variable to which it is ascribed. The AoA of a LOS wave is assumed to be uniformly distributed over the unit half-sphere, while the angle α defining the direction of polarization vector (5) is uniformly distributed on the unit circle. The angles θ, ϕ and α are statistically independent. They can be

generated as the random variables

$$\theta^u = \text{acos}(1 - 2p_\theta), \tag{6}$$

$$\phi^u = \pi p_\phi - \frac{\pi}{2}, \tag{7}$$

$$\alpha^u = 2\pi p_\alpha, \tag{8}$$

where $p_\theta, p_\phi, p_\alpha \in \mathcal{U}(0,1)$, i.e., they are drawn from a uniform distribution law.

2.3 The RIMP channel

In the RIMP propagation channel, the EM field impinging at the receive antenna is assumed to consist of N_{w} plane waves. Then, applying the superposition principle

$$H_{n,m}^u = \frac{c}{\sqrt{N_{\text{w}}}} \sum_{l=1}^{N_{\text{w}}} \boldsymbol{F}_n(\theta_{m,l}^u, \phi_{m,l}^u) \cdot \hat{\boldsymbol{p}}_{m,l}^u \text{e}^{j\varphi_{m,l}^u}, \tag{9}$$

where $c = 1$ can be assumed. The polarization vector of the wave arriving from direction $(\theta_{m,l}^u, \phi_{m,l}^u)$ is given by

$$\hat{\boldsymbol{p}}_{m,l}^u = \sin(\alpha_{m,l}^u)\hat{\boldsymbol{\theta}} + \cos(\alpha_{m,l}^u)\hat{\boldsymbol{\phi}}, \tag{10}$$

The angle $\theta_{m,l}$ is obtained from (6). The angles $\phi_{m,l}$ and $\alpha_{m,l}$ and the phase $\varphi_{m,l}$ are obtained from (7) and (8), respectively. The realizations of these random variables are statistically independent.

2.4 MIMO efficiency

A fundamental QoS parameter of a wireless system is throughput. It has bee shown previously that in LTE/LTE-A systems the throughput can be modelled by the ideal digital threshold receiver model [10]. Hence, the relative throughput can be expressed by the Probability of Detection (PoD) curves of single or multiple bitstreams. For a single data bitstream the PoD is given by

$$\text{PoD}\left(\gamma_{\text{av}}\right) = \frac{T_{\text{put}}\left(\gamma_{\text{av}}\right)}{T_{\text{put,max}}} = 1 - \text{CDF}\left(\frac{\gamma_{\text{th}}}{\gamma_{\text{av}}}\right), \tag{11}$$

where $\text{CDF}\left(\frac{\gamma_{\text{th}}}{\gamma_{\text{av}}}\right)$ is the Cumulative Distribution Function of the average SNR after digital processing and γ_{av} is receive power. γ_{th} denotes the receiver threshold level. The former defines the minimum signal SNR for successful data transmission, which can achieve maximum throughput in the AWGN channel. In order to evaluate the data throughput,
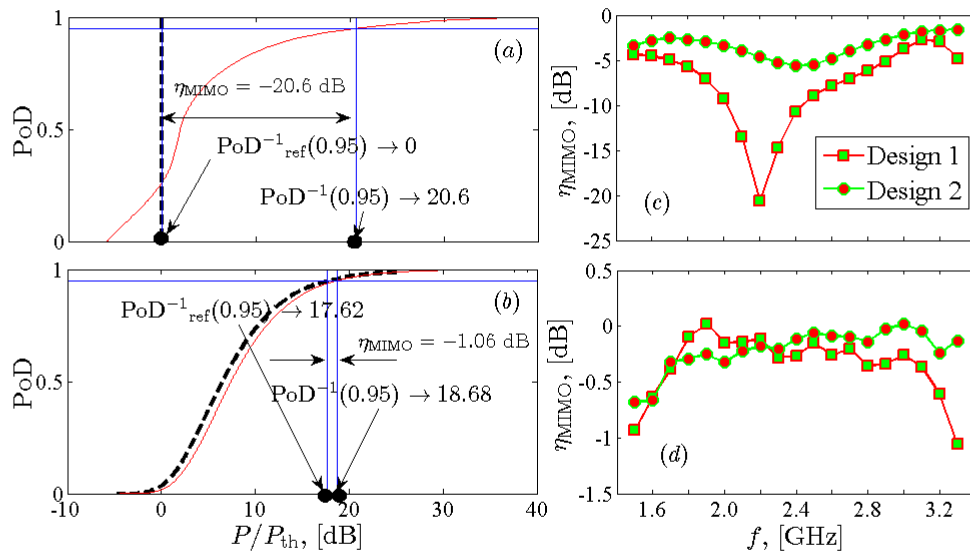
Figure 1: (a) and (b) show examples of PoD curves and the derived MIMO efficiencies, (c) and (d) show the MIMO efficiency as function of frequency in RLOS and RIMP, respectively. The antenna designs are described in [11].

the data stream with the smallest SNR at the output of the MIMO receive antenna is computed according to

$$\gamma_{\mathrm{av}} = \min(\gamma_1^{\mathrm{ZF}}, \gamma_2^{\mathrm{ZF}}, \ldots, \gamma_{N_{\min}}^{\mathrm{ZF}}), \qquad (12)$$

where $N_{\min} = \min\{N_r, N_t\}$. The MIMO efficiency can then be defined based on the 95% throughput level as

$$\eta_{\mathrm{MIMO}} = \frac{\mathrm{PoD}_{\mathrm{ref}}^{-1}(0.95)}{\mathrm{PoD}^{-1}(0.95)}, \qquad (13)$$

where $\mathrm{PoD}^{-1}(0.95)$ and $\mathrm{PoD}_{\mathrm{ref}}^{-1}$ denote the inverse function of the PoD computed (or measured) at the 0.95 PoD-level corresponding to the characterized antenna and the reference antenna, respectively.

2.5   Numerical results and analysis

Fig. 2 shows the MIMO efficiency (13) computed for two antenna designs denoted 1 and 2 (these correspond to the early and the new designs, respectively, presented in [11]). For the RIMP simulations it was assumed that the number of waves $N_{\mathrm{w}} = 100$. A number of 10^5 independent realizations was chosen to generate both the RIMP and RLOS simulations. Fig. 2(a) shows the computed PoD function for antenna design 1 in RLOS at $f = 2.2$ GHz. Fig. 2(b) shows the PoD for the same antenna in RIMP and $f = 3.3$ GHz. Fig. 2(c) and (d) show the MIMO efficiency as a function of operating frequency for both antenna designs in RLOS and RIMP, respectively. As can be seen from Fig. 2(c) and (d),

the MIMO efficiency of an antenna is not necessarily similar in different environments. The insufficient system throughput performance due to antenna design 1 in RLOS was eradicated by the antenna design 2. Good performance in RIMP was preserved by antenna design 2 over an octave bandwidth.

The presented MIMO efficiency analysis is general and can be employed to evaluate the performance of antennas and devices in 4G communications systems or any other system that can be described by the ideal digital threshold receiver model [12–15]. The presented approach allows to identify the reasons leading to performance degradation in wireless channels based on the performance of two limiting propagation channels, i.e., the RIMP and the RLOS channels as presented in [11, 17]. Furthermore, the performance analysis allows for a straightforward inclusion of the randomness of propagation channels induced by the user [18, 19]. In a practical OTA set-up measurement errors will directly impact the MIMO efficiency.

3 Massive MIMO

3.1 System Model

Let's now consider the downlink of a single-cell narrowband Massive MIMO system. Also assumed is an RBS (radio base station) comprising M antenna elements with equal number of ports, which is serving K single-antenna users, or user equipment (UE), where $M \geq K$. Let $\mathbf{x} \in \mathbb{C}^{M \times 1}$ denote the signal vector transmitted from the RBS antenna array with normalized power $E\{\|\mathbf{x}\|^2\} = 1$. The operation $E\{\|\mathbf{x}\|^2\}$ denotes the expected value of $\|\mathbf{x}\|^2$, where $\|\mathbf{x}\|$ is the Euclidean norm of the complex vector $\mathbf{x}$.

The vector containing the receive signal of the K UEs $\mathbf{y} \in \mathbb{C}^{K \times 1}$ can be expressed as

$$\mathbf{y} = \sqrt{\mathsf{SNR}_{\mathrm{dl}}}\mathbf{H}\mathbf{x} + \mathbf{n}, \tag{14}$$

where $\mathsf{SNR}_{\mathrm{dl}}$ is the average per-UE signal-to-noise ratio (SNR); we dont use the subscript in the following. $\mathbf{n} \in \mathbb{C}^{K \times 1}$ is the noise vector containing the Additive White Gaussian Noise (AWGN) components at each UE, which we assume here to have unit variance. $\mathbf{H} \in \mathbb{C}^{K \times M}$ is the downlink Massive MIMO channel matrix satisfying the normalization $E\{|H_{k,m}|^2\} = 1$.

3.2 The RLOS channel

We assume that the receive antenna of the kth UE and the mth transmit antenna element of the massive uniform linear array are in the far-field of each other. Their situations are

given by $\boldsymbol{r}_k$ and $\boldsymbol{r}_m$, respectively. Hence, the coupling between the two antennas can be computed as

$$H_{k,m} = \alpha_1 \boldsymbol{F}_m(\hat{\boldsymbol{r}}_{km}) \cdot \boldsymbol{F}_k(-\hat{\boldsymbol{r}}_{km}) \frac{e^{-j\frac{2\pi}{\lambda}|\boldsymbol{r}_k - \boldsymbol{r}_m|}}{|\boldsymbol{r}_k - \boldsymbol{r}_m|}, \tag{15}$$

where λ is the wavelength corresponding to the operating frequency, $\boldsymbol{F}_m(\hat{\boldsymbol{r}}_{km})$ is the far-field function of the embedded array antenna element with index m when referred to the phase reference point $\boldsymbol{r}_m$ of that element and transmitting in direction $\hat{\boldsymbol{r}}_{km} = (\boldsymbol{r}_k - \boldsymbol{r}_m)/|\boldsymbol{r}_k - \boldsymbol{r}_m|$. The far-field function of the kth UE is given by $\boldsymbol{F}_k(-\hat{\boldsymbol{r}}_{km})$. The constant α_1 is obtained from the channel matrix normalization given above. The randomness is assumed to be due to various reasons, first, the kth UE's position, $\boldsymbol{r}_k$, is random over the coverage area, and secondly, the far-field functions orientation of the kth UE, $\boldsymbol{F}_k$, changes from position to position due to the user's movement.

3.3 The RIMP channel

In RIMP, in addition to the assumption that transmit and receive antennas are in each others far-fields, we assume that the scatterers and the antennas are in each others far-field too. The position of the ith scatterer associated with the kth UE are denoted as $\boldsymbol{r}_{i,k}$. The coupling between the two antennas can be then expressed as

$$H_{k,m} = \alpha_2 \sum_{i=1}^{N_{\text{sc}}} \boldsymbol{F}_m(\hat{\boldsymbol{r}}_{i,k}) \cdot \boldsymbol{E}_{i,k}(-\hat{\boldsymbol{r}}_{i,k}), \tag{16}$$

where λ denotes the wavelength, $\boldsymbol{F}_m(\hat{\boldsymbol{r}}_{i,k})$ is the far-field function of the embedded array antenna element of index m when referred to the phase reference point $\boldsymbol{r}_m$ of that element and radiating in direction $\hat{\boldsymbol{r}}_{i,k}$. The far-field function of the scattered field associated with the kth UE is given by the complex vector $\boldsymbol{E}_{i,k}(-\hat{\boldsymbol{r}}_{i,k})$, which has random amplitude, phase and polarization. The constant α_2 is obtained from the channel matrix normalization given above.

3.4 Ergodic sum-rate and capacity loss

We assume perfect CSI (Channel State Information) at both the receiver and the transmitter. The transmit signal from the M antennas, $\mathbf{x}$, is a linear combination of the symbols intended for the K UEs. The symbol intended for the kth UE q_k, such that $E\{|q_k|^2\} = 1$. Thus, the linearly precoded transmit signal vector $\mathbf{x}$ can be expressed as

$$\mathbf{x} = \sqrt{\beta}\mathbf{W}\mathbf{q}, \tag{17}$$

where $\mathbf{q} \in \mathbb{C}^{K \times 1}$, $\mathbf{W} \in \mathbb{C}^{M \times K}$ is the precoding matrix, and $\beta = 1/E\{\mathrm{tr}(\mathbf{W}\mathbf{W}^H)\}$ is a normalization constant chosen to satisfy the power constraint $E\{\|\mathbf{x}\|^2\} = 1$.

Next we consider the Zero-Forcing (ZF) precoding and the Matched-Filtering (MF) precoding also known as Maximum Ratio Transmission (MRT). The precoding matrix is then given by

$$\mathbf{W} = \begin{cases} \mathbf{H}^\dagger & \text{for MF,} \\ \mathbf{H}^\dagger(\mathbf{H}\mathbf{H}^\dagger)^{-1} & \text{for ZF.} \end{cases} \tag{18}$$

The signal-to-interference-plus-noise ratio (SINR) of the kth UE in the downlink, i.e., the kth-bitstream, can be computed as

$$\mathsf{SINR}_k = \frac{\beta\mathsf{SNR}|\mathbf{H}_{k:}\mathbf{W}_{:k}|^2}{\beta\mathsf{SNR}\sum_{k'\neq k}^K |\mathbf{H}_{k:}\mathbf{W}_{:k'}|^2 + 1}, \tag{19}$$

where $\mathbf{H}_{k:}$ is the kth row of matrix $\mathbf{H}$ and $\mathbf{W}_{:k}$ is the kth column of matrix $\mathbf{W}$.

The ergodic sum-rate of the $(M \times K)$ Massive MIMO system is

$$\mathsf{SR} = \sum_{k=1}^K E\{\log_2(1 + \mathsf{SINR}_k)\}, \tag{20}$$

where SINR_k is the SINR of the kth UE computed above.

3.5 Capacity loss

The deficient antennas or antennas with errors are simulated assuming that a number $N_{\text{ant. in loss}} < M$ of antenna elements have a total embedded radiation efficiency that is less than 100%. The index l of the deficient antenna elements is chosen randomly. However, to simplify this initial analysis we assume that each element has the same performance loss factor P_{loss}. Thus, the channel matrix entries corresponding to each of the $N_{\text{ant. in loss}}$ antennas chosen at random can be computed as

$$H_{k,l}^{\text{loss}} = \frac{H_{k,l}}{\sqrt{P_{\text{loss}}}}, \tag{21}$$

Now using (21) we can obtain the SINR of the kth UE when a subset of the RBS antenna elements contains deficient antennas, i.e., $\mathsf{SINR}_k^{\text{loss}}$. A capacity loss can then be defined accordingly

$$C_{\text{loss}} = 100\left(1 - \frac{\mathsf{SR}^{\text{loss}}}{\mathsf{SR}}\right), \tag{22}$$

where $\mathsf{SR}^{\text{loss}}$ and SR are the sum-rate capacities computed when some of the antennas are deficient and when all the antennas are 100% efficient, respectively.

3.6 Numerical results and analysis

The presented numerical results in this section are obtained using specific values of parameters, statistical distributions and scenarios. We assume a single-cell narrowband Massive MIMO system with operating frequency $f = 30$ GHz. The uniform linear array at the RBS is assumed to have $M = 50$ vertically polarized isotropic antenna elements separated at the distance $d = \lambda/2 = 0.005$ m. The size of the array is determined as $L = M\lambda/2 = 0.25$ m. For the RLOS propagation scenario we assume a horizontal $120°$ 2D sector-cell. The $K = 5$ UEs are uniformly distributed over an area covering distances to the RBS from 12.5 m to 300 m. Each UE is assumed to be equipped with an isotropic antenna. Transmit and receive antenna heights are assumed be the same since simulations are performed for users distributed over the horizontal plane only. In the RIMP case we assume that the amplitudes are all equal and the phases are uniformly distributed between 0 and 2π. The directions-of-arrival, or more correctly, the directions-of-departure, of the waves are assumed to be isotropically distributed, i.e., they are uniformly over all directions. In both RIMP and RLOS it is assumed that the orientation of the polarization vector is randomly oriented in the plane perpendicular to the direction of propagation. Therefore, the polarization mismatch between the polarization of the array antenna elements and the impinging fields has also been included in the analysis.

Fig.2 displays the capacity loss assuming MRF precoding in RLOS as a function of the number of deficient antennas (i.e., antennas in loss) $N_{\text{ant. in loss}} < M$ for different values of the performance loss factor P_{loss}. Three average per-UE SNR values have been considered for illustrative purpose: 0 dB, 10 dB and 20 dB shown in the left, middle and right subplots, respectively. Fig.3 demonstrate similar results for the ZF precoding. Fig.4 and Fig.5 show analogous results to Fig.2 and Fig.3, respectively, for the RIMP channel in this case.

The following observations can be made from the results presented above. The first, most obvious, result is that the capacity loss due to lower antenna efficiency, or higher error, increases with both the number of deficient antennas and the power loss. Clearly, the antenna element deficiency translates into both "effectively" smaller arrays and arrays with "effectively" less elements. Hence, since the sum-rate capacity of Massive MIMO decreases as the ratio M/K decreases we then have an increase in capacity loss. The largest capacity losses are observed for the RLOS as compared to RIMP. This leads to the observation that the deficient antennas have a major impact on system performance in RLOS channels due to less efficient use antenna elements at the RBS. The smaller beamforming gain due to the smaller number of effectively contributing antenna elements results in lower per-UE SINR. A similar trend is observed when we compare MRF and
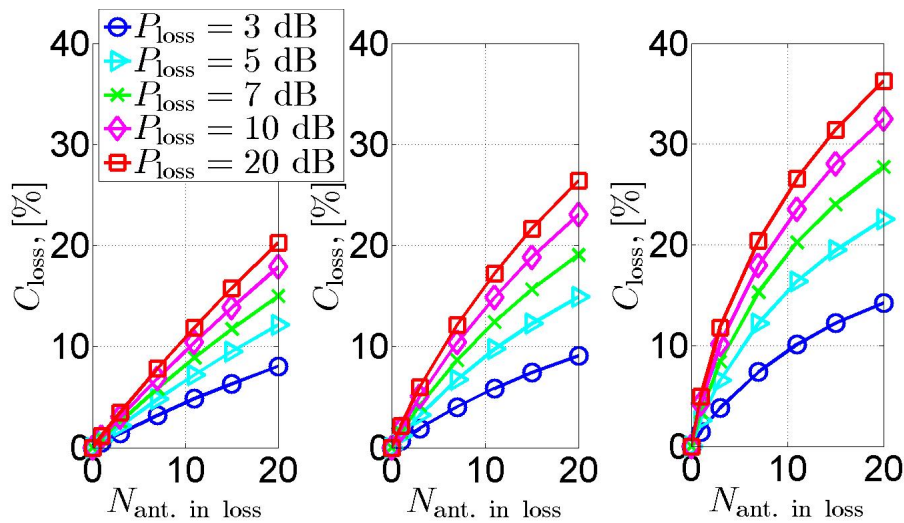
Figure 2: Capacity loss for the MRF precoding in RLOS as a function of the number of deficient antennas $N_{\text{ant. in loss}}$ for different values of the performance loss factor P_{loss}. Results are presented for three average per-UE SNR values: 0 dB, 10 dB and 20 dB shown in the left, middle and right subplots, respectively,
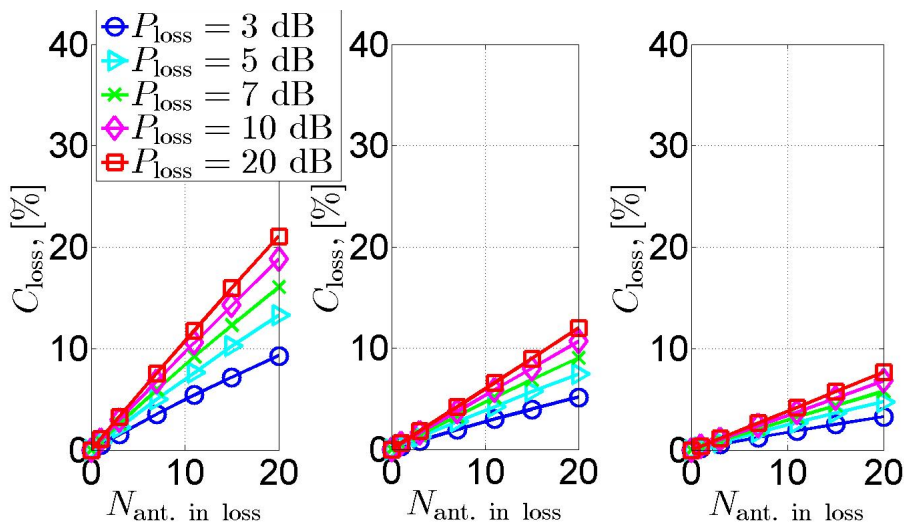

Figure 3: Capacity loss for the ZF precoding in RLOS as a function of the number of deficient antennas $N_{\text{ant. in loss}}$ for different values of the performance loss factor P_{loss}. Results are presented for three average per-UE SNR values: 0 dB, 10 dB and 20 dB shown in the left, middle and right subplots, respectively

ZF, since the former is more dependent on the actual SINR maximization as compared to ZF, which relies on interference mitigation. We clearly see that both the RIMP and
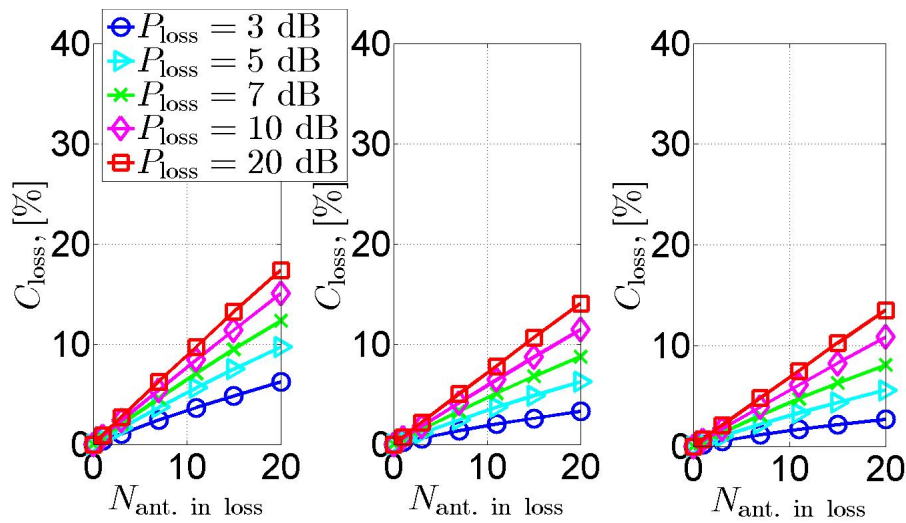
Figure 4: Capacity loss for the MRF precoding in RIMP as a function of the number of deficient antennas $N_{\text{ant. in loss}}$ for different values of the performance loss factor P_{loss}. Results are presented for three average per-UE SNR values: 0 dB, 10 dB and 20 dB shown in the left, middle and right subplots, respectively
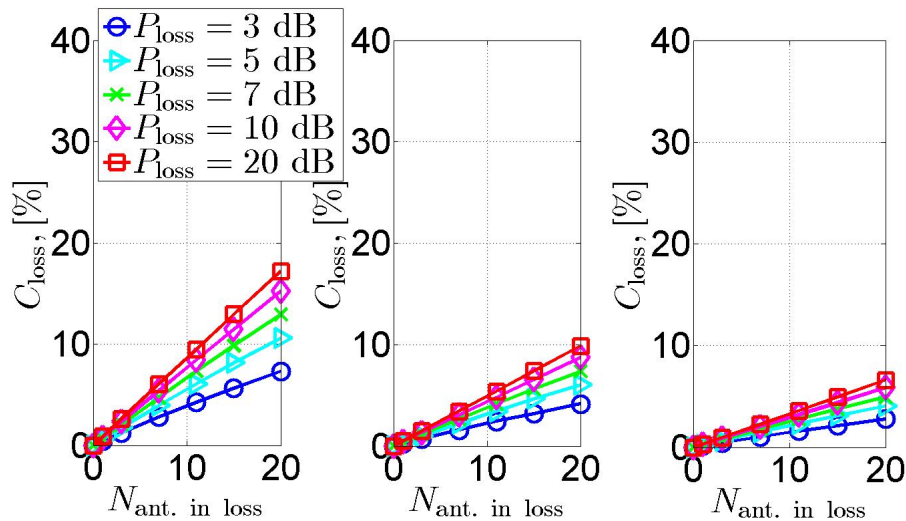

Figure 5: Capacity loss for the ZF precoding in RIMP as a function of the number of deficient antennas $N_{\text{ant. in loss}}$ for different values of the performance loss factor P_{loss}. Results are presented for three average per-UE SNR values: 0 dB, 10 dB and 20 dB shown in the left, middle and right subplots, respectively

the RLOS can be used to identify deficient performance of Masive MIMO arrays for ideal linear precoders such as the ZF and the MRF precoders.

The results presented in this deliverable have addressed the requirement of Task 2.2 in the is3DMIMO project. In the future, more results will be delivered to contribute to the comparison of the 3D SMX and 3D beamforming performance obtained under the indoor 3D SCME MIMO channel model established in Task 1.2 and that under the measured indoor 3D MIMO channel in Task 1.3.

4 Conclusions

It has been shown that ZF and MRF linear precoding is more sensitive to antenna element deficiency in terms of poor, or erroneous characterization of, total embedded efficiency in the RLOS channel than in the RIMP channel. This is of a great relevance to the design of Massive MIMO systems at 5G mmWave frequency bands. As the antenna element deficiency results in both "effectively" smaller arrays and arrays with "effectively" less elements the performance of MRF is more sensitive to poor antenna efficiency than ZF. The MRF relies more on link gain maximization than ZF that relies on interference cancellation. Finally, we have shown that both the RIMP and the RLOS can be used to identify deficient performance of Massive MIMO arrays employing ZF and MRF precoding.

Hence, Over-the-Air (OTA) measurements and characterization of Massive MIMO antenna systems for 5G have can benefit from time- and cost-efficient measurement technologies based on the RIMP and the RLOS testing environments.

References

[1] T. L. Marzetta, "Noncooperative cellular wireless with unlimited numbers of base station antennas," *IEEE Trans. Wireless Commun.*, vol. 9, no. 11, pp.3590–3600, Nov. 2010.

[2] F. Rusek, D. Persson, B. K. Lau, E. G. Larsson, T. L. Marzetta, O. Edfors, and F. Tufvesson, "Scaling up MIMO: Opportunities and challenges with very large arrays," *IEEE Signal Process. Mag.*, vol. 30, no. 1, pp. 40–46, Jan. 2013.

[3] H. Q. Ngo, E. G. Larsson, and T. L. Marzetta, "Aspects of favorable propagation in massive MIMO," *in Proc. EUSIPCO*, 2014.

[4] E. Björnson, E. G. Larsson, and T. L. Marzetta, "Massive MIMO: 10 myths and one grand question, *arXiv preprint* arXiv:1503.06854, Mar. 2015.

[5] X. Gao, O. Edfors, F. Rusek, F. Tufvesson, "Massive MIMO Performance Evaluation Based on Measured Propagation Data," in *Wireless Communications, IEEE Transactions on* , vol.14, no.7, pp.3899-3911, July 2015.

[6] A. A. Glazunov, S. M. Moghaddam and J. Yang, "Simulating the MIMO efficiency of antennas," *In Proc. ISAP 2017*, Phuket, pp. 1-2.

[7] A. A. Glazunov, "Impact of Deficient Array Antenna Elements on Downlink Massive MIMO Performance in RIMP and Random-LOS Channels," in *In Proc. EuCAP2018*, London, pp. 1-4.

[8] P.-S. Kildal, "Rethinking the Wireless Channel for OTA testing and Network Optimization by Including User Statistic: RIMP, Pure-LOS, Throughput and Detection Probability," *In Proc. ISAP 2013*, Nanjing, pp. 1-4.

[9] P. S. Kildal, A. A. Glazunov, J. Carlsson and A. Majidzadeh, "Cost-effective measurement setups for testing wireless communication to vehicles in reverberation chambers and anechoic chambers," *In Proc. IEEE CAMA 2014*, Antibes Juan-les-Pins, pp. 1-4.

[10] P.-S. Kildal, *et al.*, "Threshold Receiver Model for Throughput of Wireless Devices With MIMO and Frequency Diversity Measured in Reverberation Chamber," *IEEE AWPL*, vol. 10 pp. 1201-1204, 2011.

[11] S. M. Moghaddam, *et al.*, "Improvement of an Octave Bandwidth Bowtie Antenna Design Based on the Analysis of a MIMO Efficiency Metric in Random-LOS," *Microwave and Optical Technology Letters*, Vol. 59, No. 6, pp. 1229-1233, 2017.

[12] A. Hussain, P. S. Kildal and A. A. Glazunov, "Interpreting the Total Isotropic Sensitivity and Diversity Gain of LTE-Enabled Wireless Devices From Over-the-Air Throughput Measurements in Reverberation Chambers," in *IEEE Access*, vol. 3, pp. 131-145, 2015.

[13] M. S. Kildal, *et al.*, "Initial measured OTA throughput of 4G LTE communication to cars with roof-mounted antennas in 2D random-LOS," *In Proc. ISAP 2015*, Hobart, TAS, pp. 1-4.

[14] S. M. Moghaddam, A. A. Glazunov, J. Yang and M. Gustafsson, "Semi-omnidirectional dual-polarized wideband multiport antennas for MIMO applications in Random-LOS and RIMP," *In Proc. EuCAP 2017*, Paris, France, 2017, pp. 636-639.

[15] J. Yang and A. A. Glazunov, "Design and characterization of cost-effective planar antennas with steerable beams: Gap waveguides, SMT and random-LOS," *In Proc. ISAP 2016*, Okinawa, pp. 116-117.

[16] D. S. Prinsloo, *et al.*, "Synergy in design of phased array antennas for modern radio astronomy and wireless communication systems," *In Proc. EuCAP 2016*, Davos, pp. 1-5.

[17] A. Razavi, A. A. Glazunov, P. S. Kildal and J. Yang, "Characterizing Polarization-MIMO Antennas in Random-LOS Propagation Channels," in *IEEE Access*, vol. 4, pp. 10067-10075, 2016.

[18] P. H. Lehne, *et al.*, "Measuring user-induced randomness to evaluate smart phone performance in real environments," *In Proc. EuCAP 2015*, Lisbon, pp. 1-5.

[19] A. A. Glazunov and P. H. Lehne, "A Spherical Probability Distribution Model of the User-Induced Mobile Phone Orientation," *in IEEE Access*, vol. 6, pp. 37185-37194, 2018.